

ANALYTICAL SOLUTION FOR POTENTIAL FLOW AROUND A ROTATING SPHERE AND COMPARISON WITH CFD

Tariq ALMIQASBI¹, Ekrem YILMAZ², Aydın ŞALCI³

¹Mechanical Engineering Department, Altınbaş University, Türkiye, tarek1392005@gmail.com
(<https://orcid.org/0009-0007-0261-7791>)

²Mechanical Engineering Department, Altınbaş University, Türkiye, ekrem.yilmaz1@altinbas.edu.tr
(<https://orcid.org/0000-0002-4075-219X>)

³Mechanical Engineering Department, Altınbaş University, Türkiye, aydin_salci@gmail.com
(<https://orcid.org/0000-0002-2040-7591>)

Received: 23.01.2024

Accepted: 27.02.2024

Published: 30.06.2024

*Corresponding author

Research Article

pp.101-111

DOI: 10.53600/ajesa.1424673

Abstract

A three-dimensional analytical solution was derived for an incompressible steady potential at an initially uniform velocity flow around a sphere, which translates forward, backward, rotates longitudinally or transversally. The concept of relative velocity was used to analyze the flow around the transitionally moving sphere. To analyze the flow around the longitudinally rotating sphere, A formula of the circumferential velocity of the fluid is found at the equatorial plane of the sphere and then generalized to the whole sphere as an approximation. The superposition principle of velocities was used to analyze the flow around the transversely rotating sphere, the stagnation points were detected and analyzed, the pressure distribution at the equator was calculated and compared with the experimental and CFD results, and the lift coefficient was calculated and compared with the experimental results and a good agreement for C_p and C_L was found at low spin factors, In contrast, at high spin factors the results begin to diverge due to the viscous effects and eddy formation.

Keywords: Potential flow, analytical solution, rotating sphere, superposition principle, stagnation points

POTANSİYEL AKIŞ İÇİN DÖNEN BİR KÜRE ANALİTİK ÇÖZÜMLEME VE CFD İLE KARŞILAŞTIRILMASI

Özet

İleriye veya geriye doğru hareket eden veya uzunlamasına veya enlemesine dönen bir küre etrafında başlangıçta tekdüze bir hız akışındaki sıkıştırılamaz sabit potansiyel için üç boyutlu bir analitik çözüm türetildi; geçişli olarak hareket eden küre etrafındaki akışı analiz etmek için bağıl hız kavramı kullanıldı. . Boyuna dönen küre etrafındaki akışı analiz etmek için, kürenin ekvator düzleminde akışkanın çevresel hızının bir formülü bulunur ve daha sonra bir yaklaşım olarak tüm küreye genelleştirilir. Enine dönen küre etrafındaki akışı analiz etmek için hızların süperpozisyon prensibi kullanılmış, durma noktaları tespit edilip analiz edilmiş, ekvatordaki basınç dağılımı hesaplanıp deneysel ve CFD sonuçlarıyla karşılaştırılmış, kaldırma katsayısı hesaplanıp karşılaştırılmıştır. düşük spin faktörlerinde C_p ve C_L için iyi bir uyumun olduğu, yüksek spin faktörlerinde ise viskoz etkiler ve girdap oluşumu nedeniyle sonuçlar farklılık göstermeye başladığı görülmüştür.

Anahtar Kelimeler: Potansiyel akış, analitik çözüm, dönen küre, süperpozisyon prensibi, durgunluk noktaları

1. Introduction

Understanding the flow of fluids around rotating spheres is crucial in various scientific and engineering fields due to its diverse applications. While potential flow theory simplifies the problem by assuming an ideal, inviscid fluid without friction, it provides valuable insights into real-world fluid dynamics.

Spinning sports balls (football, golf, baseball, tennis) experience lift and drag due to the Magnus effect, where the rotation interacts with the surrounding airflow. Potential flow models provide a basic understanding of this phenomenon [7].

Potential flow models provide intuitive visualizations of streamlines and pressure distributions around the sphere, revealing how rotation affects the flow patterns.

Unlike viscous flow problems, potential flow around a rotating sphere often admits analytical solutions. These solutions offer valuable mathematical tools for understanding the basic dynamics and developing further theoretical models.

The analytical solution for an incompressible viscous flow is constricted in simple geometries and unidirectional flows, where the difficult nonlinear convective terms in momentum equations were omitted, whereas the potential flow is not constricted to these cases because they are canceled for inviscid flows[4, p. 529].

1.1. The Potential Flow Around a Rotating Cylinder

White [4, p.546-548] and Anderson [3, sec.3.15] derived a two-dimensional analytical solution for an incompressible steady potential at an initially uniform velocity flow around a rotating cylinder, a stream function is used as a summation of three types: a uniform, a doublet, and a vortex, the equations of radial and tangential velocities were obtained [4, eq. 8.38] [3, eqs. 3.119-3.120].

The three-dimensional flow around a rotating cylinder can be considered as two-dimensional flow due to the axial symmetry, then the stream function is used because it's restricted to two-dimensional flows, it can't be used in the three-dimensional flows [4, p. 264], for this reason the stream function cannot be used in the three-dimensional flows around rotating spheres.

Anderson [3] in his book investigated in detail the potential flow around a non-rotating cylinder and a transversely rotating cylinder, he derived expressions for the pressure coefficients for the two previous cases.

1.2. The Potential Flow Around a Rotating Sphere

Graebel [8, sec 2.4], and White [4, sec 8.8] wrote in detail in potential flows, he stated that if a sphere is accelerated in an inviscid fluid, there will be a drag pressure exerted on the sphere, and there is an "added mass" that must be considered in writing Newton's second law, and if the sphere moves at a constant velocity in an inviscid fluid, there is no drag pressure exerted on the sphere, then there is no need to use "added mass".

Briggs [2] measured experimentally the effect of the angular velocity and the velocity of the air stream on the lateral deflection of a baseball by dropping the baseball while rotating around a vertical axis through a horizontal wind stream in a tunnel, he also measured experimentally the pressure distribution in the equatorial plane of a smooth and rough Bakelite spinning spheres, the ball diameter was 3-in (0.0381m), the wind speed was 125 ft/s (38.1 m/s), and the angular velocity was 1800 rpm (188.5 rad/s), he represented his results graphically.

Alaways and Hubbard [5] developed a theoretical model for determining the lift force on spinning spheres, They used the (unpublished data) of Sycorsky and Lightfoot to compare, which measured the Magnus lift on a spinning baseball using a wind tunnel, they used three speeds of wind stream, and measured the Magus lift for both 2-seam and 4-seam orientations, the following Figure [6, Fig.1] (Figure (1)) shows the difference between two-seam and four-seam orientations.

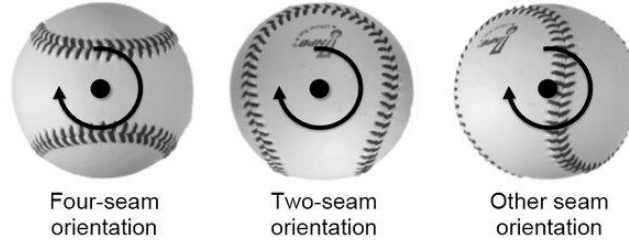


Figure 1. The difference between two-seam and four-seam orientations.

1.3. The Potential Flow Around A Fixed Sphere

Hildebrand [1, Sec. 9.8] solved this problem which is an initially uniform flow passes a fixed sphere, this flow is downward, see Figure 2, the flow is axisymmetric about the z-axis, there is no circumferential velocity component, the flow is an incompressible, steady, and potential (an inviscid and an irrotational), he used the governing differential equation:

$$\frac{\partial}{\partial R} \left(R^2 \frac{\partial \phi}{\partial R} \right) + \frac{1}{\sin \varphi} \frac{\partial}{\partial \varphi} \left(\sin \varphi \frac{\partial \phi}{\partial \varphi} \right) = 0 \quad (1)$$

By using the separation of variables method, the Legendre solution, and the boundary conditions:

$$V_R(a, \varphi) = 0 \quad (2)$$

$$\lim_{R \rightarrow \infty} \mathbf{V} = -U_{\infty} \mathbf{k} \quad (3)$$

He obtained the solution and the velocity:

$$\phi(R, \varphi) = -U_{\infty} \left(R + \frac{1}{2} \frac{a^3}{R^2} \right) \cos \varphi + C \quad (4)$$

$$\mathbf{V} = -U_{\infty} \left[1 - \left(\frac{a}{R} \right)^3 \right] \cos \varphi \mathbf{e}_R + U_{\infty} \left[1 + \frac{1}{2} \left(\frac{a}{R} \right)^3 \right] \sin \varphi \mathbf{e}_{\varphi} \quad (5)$$

2. Methods

2.1. Spherical Coordinates

In spherical coordinates [9] the point P in space is determined by three components (R, φ , θ), as illustrated in Figure 2.

2.1.1. The Spherical Coordinates With Different Orientation

The spherical coordinates with different orientation, in which the x-axis points upward, shown in the Figure 3.

A correspondence between Figure 1 and Figure 2 leads to

$$\cos \bar{\varphi} = \sin \varphi \cos \theta \quad (6)$$

$$\cos \bar{\theta} = \frac{\sin \varphi \sin \theta}{\sqrt{1 - \sin^2 \varphi \cos^2 \theta}} \quad (7)$$

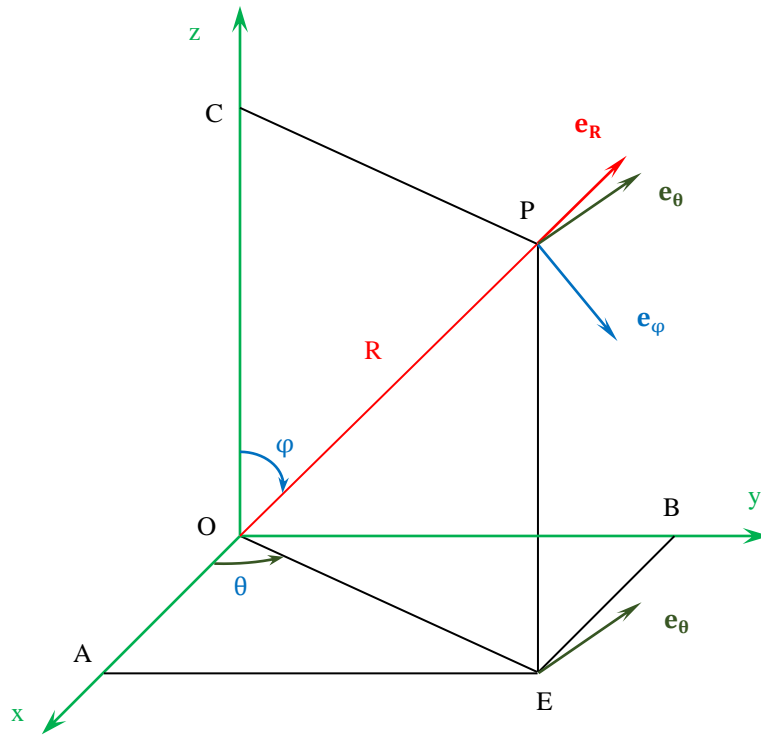


Figure 2. The spherical coordinates.

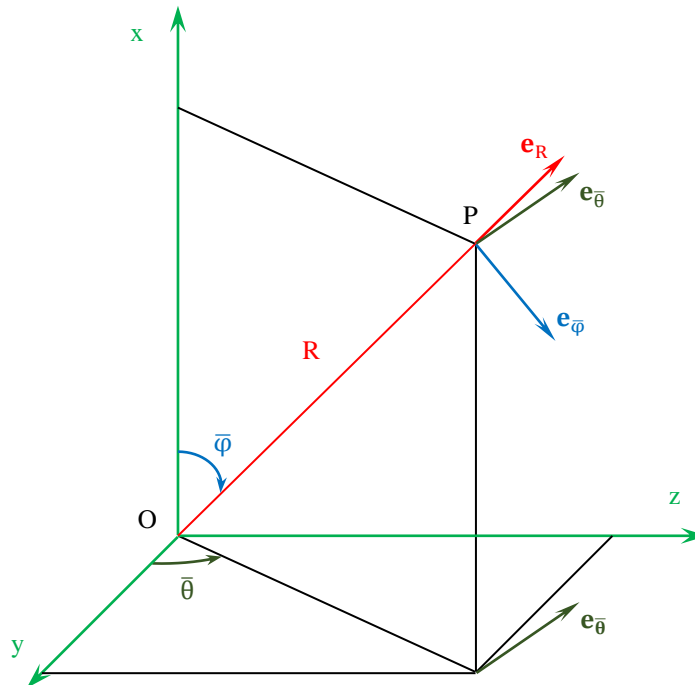


Figure 3. The spherical coordinates with different orientation.

$$\sin \bar{\theta} = \frac{\cos \varphi}{\sqrt{1 - \sin^2 \varphi \cos^2 \theta}} \quad (8)$$

2.2. Potential Flow Around A Longitudinally Rotating Sphere

If the sphere described earlier in section 2.3 rotates longitudinally with an angular velocity of ω (rad/s) around z-axis in the direction of the increasing of angle θ , see figure 2, the flow will still axisymmetric about the z-axis, and the governing equation (Equation 1) will still valid, by following the same procedure in section 2.3 and adding a boundary condition by assuming that the circumferential velocity of the fluid at the equator of the sphere equals the circumferential velocity of the rotating sphere itself at the same place, i.e.

$$V_{\theta} \left(a, \frac{\pi}{2} \right) = \omega a \quad (9)$$

The obtained solution will be

$$\phi(R, \varphi, \theta) = -U_{\infty} R \left[1 + \frac{1}{2} \left(\frac{a}{R} \right)^3 \right] \cos \varphi + \omega a^2 \theta + C \quad (10)$$

$$\mathbf{v} = -U_{\infty} \left[1 - \left(\frac{a}{R} \right)^3 \right] \cos \varphi \mathbf{e}_R + U_{\infty} \left[1 + \frac{1}{2} \left(\frac{a}{R} \right)^3 \right] \sin \varphi \mathbf{e}_{\varphi} + \frac{\omega a^2}{R \sin \varphi} \mathbf{e}_{\theta} \quad (11)$$

2.3. Potential Flow Around A Transversal Rotating Sphere

If the flow described earlier in the previous section changes to flow in the opposite direction of the x-axis instead of z-axis, the sphere will rotate transversally, by using the Figure 2, Figure 3, the relations (6), (7) and (8) analyzing of velocities and the superposition principle, the velocity components becomes

$$V_R = -U_{\infty} \left[1 - \left(\frac{a}{R} \right)^3 \right] \sin \varphi \cos \theta \quad (12)$$

$$V_{\varphi} = -U_{\infty} \left[1 + \frac{1}{2} \left(\frac{a}{R} \right)^3 \right] \cos \varphi \cos \theta \quad (13)$$

$$V_{\theta} = U_{\infty} \left[1 + \frac{1}{2} \left(\frac{a}{R} \right)^3 \right] \sin \theta + \frac{\omega a^2}{R \sin \varphi} \quad (14)$$

2.3.1. The Stagnation Points

2.3.1.1. The Stagnation Points On The Sphere Surface

The stagnation occurs at two semi-circular curves, the equations of them are

$$\sin \varphi = \frac{2}{3} S \quad \theta = 270^\circ, 0^\circ \leq \varphi \leq 180^\circ, 0 \leq S \leq 1.5 \quad (15)$$

$$\sin \theta = -\frac{2}{3} S \quad \varphi = 90^\circ, 180^\circ \leq \theta \leq 360^\circ, 0 \leq S \leq 1.5 \quad (16)$$

where S is the spin parameter [5]

$$S = \frac{\omega a}{U_{\infty}} \quad (17)$$

2.3.1.2. The Stagnation Curves That Far From The Sphere Surface

The equation of stagnation curve is

$$\sin \varphi = S \frac{r^2}{\left[r^3 + \frac{1}{2} \right]} \quad (18)$$

Where

$$r = \frac{R}{a} \quad (19)$$

2.3.2. The Pressure At The Sphere Surface and Magnus-Robins Force

The pressure at the sphere surface is derived, the equation is

$$P_s - P_{\infty} = \frac{1}{2} \rho \left(U_{\infty}^2 - \frac{9}{4} U_{\infty}^2 \cos^2 \varphi \cos^2 \theta - \frac{9}{4} U_{\infty}^2 \sin^2 \theta - 3 \frac{U_{\infty} \omega a \sin \theta}{\sin \varphi} - \frac{\omega^2 a^2}{\sin^2 \varphi} \right) \quad (20)$$

The pressure coefficient equation is

$$C_p = 1 - \frac{9}{4} \cos^2 \varphi \cos^2 \theta - \frac{9}{4} \sin^2 \theta - 3 \frac{\omega a \sin \theta}{U_{\infty} \sin \varphi} - \frac{\omega^2 a^2}{U_{\infty}^2 \sin^2 \varphi} \quad (21)$$

C_p at the equatorial plane

$$C_p = 1 - \left(\frac{3}{2} \sin \theta + S \right)^2 \quad (22)$$

C_p at the equatorial plane of fixed sphere

$$C_p = 1 - \frac{9}{4} \sin^2 \theta \quad (23)$$

The Magnus-Robins force equation is

$$F = 3\pi \rho a^3 \omega U_{\infty} \quad (24)$$

The lift coefficient is

$$C_L = 6 S \quad (25)$$

3. Results

3.1. The Comparison With The Experimental Results

3.1.1. The Comparison With The Pressure Coefficient at the equatorial plane.

Figure 4 shows the pressure distribution over a fixed sphere (equation (23)), a spinning sphere (equation (22)), a spinning rough sphere [2, Fig. 6], a spinning smooth sphere [2, Fig. 5], a cylinder [3, Eq. 3.101], and a spinning cylinder [3, Eq. 3.126]

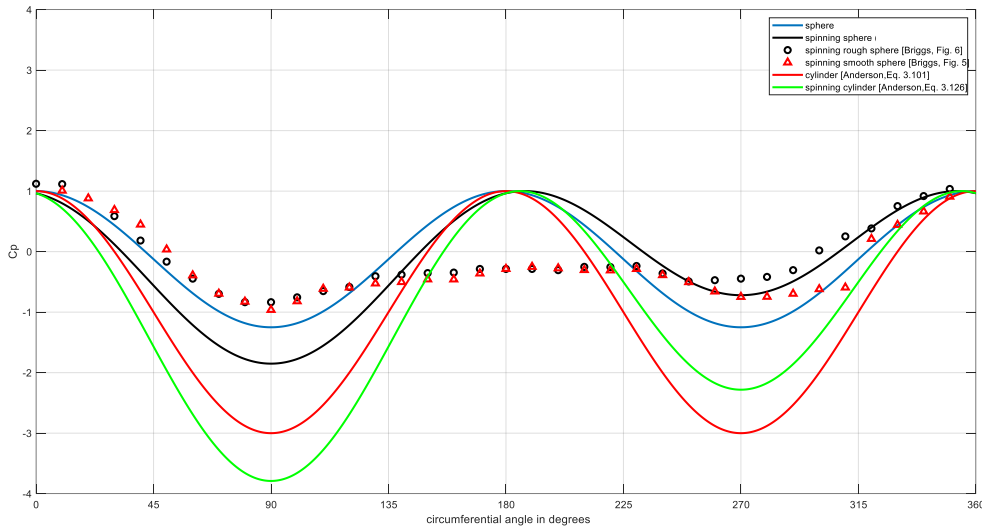


Figure 4. The Pressure Distribution Over Spheres And Cylinders.

In the experimental results, we can distinguish two tops and two bottoms, the second top is slightly flat, and the analytical curve of the spinning sphere achieves a qualitative agreement with the experimental results but differs quantitatively because of the viscous effect especially the separation process and the eddies formation at the rear side of the sphere, also the low spin factor here ($S=0.1885$) contributes in this qualitative agreement.

3.1.2. The Comparison With The Lift Coefficient

Equation (25) is presented as a red line which is plotted over the copy of Always and Hubbard figure[5, Fig. 10] as shown in Figure 5, we can see a good agreement with Sikorsky experiments on the 4-seam pitches up to nearly $S = 0.03$, if the spin parameter increases over than 0.03 the divergence will occur due to viscous effect.

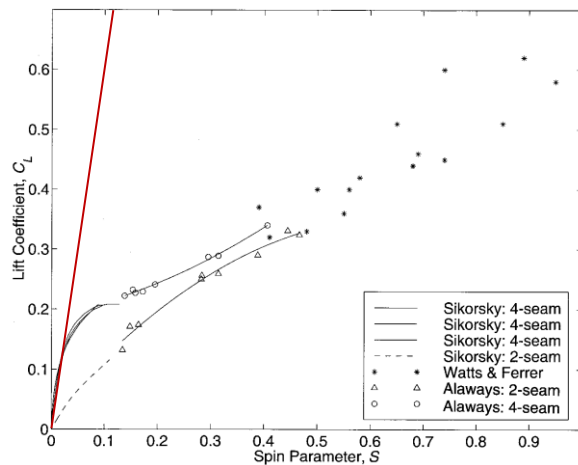


Figure 5. The Lift Coefficient Comparison With Sikorsky Experiment on The Four-Seam Baseball [5, Fig. 10].

3.2. The Comparison With The CFD Results

3.2.1. The Flow is Really Inviscid

In this sub-section, A numerical CFD solution is obtained via "FEATool Multiphysics" which is a Matlab application, to solve the Laplace equation (1) numerically, for a non-spinning sphere of a radius of 0.2 m, and $U_\infty = 1$ m/s. The flow is really inviscid because the solved Laplace equation doesn't contain viscous terms, then the resulting pressure coefficient (c_p) at the equatorial plane is plotted versus the circumferential angle (θ) in the following figure (Figure 6) with brown color, in the same figure, the analytical solution for (c_p) calculated by using Equation (23) is plotted in blue color.

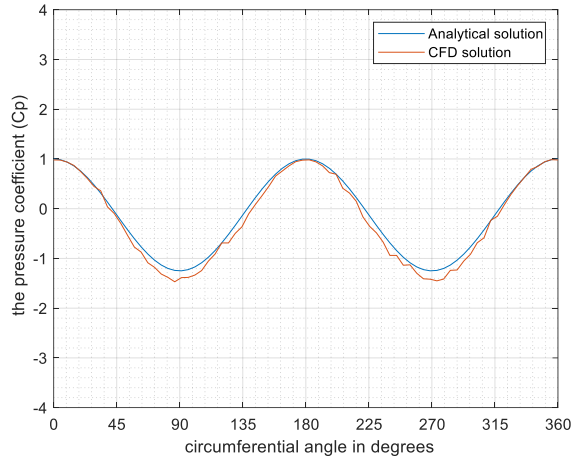


Figure 6. The Pressure Coefficient Comparison With CFD Solution For Inviscid Flow Around a Non-Spinning Sphere.

It's Obvious the very good agreement between the analytical and numerical results.

3.2.2. *The Flow has low viscosity*

In this sub-section, A numerical CFD solution is obtained via "Openfoam" to solve the low viscosity flow ($\mu = 0.001133$ kg/ms) around a sphere of a radius of 0.2 m, and $U_\infty = 1$ m/s. The flow is viscous, but for the approximation purpose, it can be considered as an inviscid, because it has a low viscosity, then the resulting pressure coefficient (c_p) at the equatorial plane is plotted versus the circumferential angle (θ) in the following figures (Figures 7-10) with blue color, in the same figure, the analytical solution for (c_p) calculated by using Equation (22) is plotted in red color, the results was obtained for non-rotating sphere and for rotating spheres with angular velocities of 1,2,5rad/s, see Figures 7 to 10, respectively.

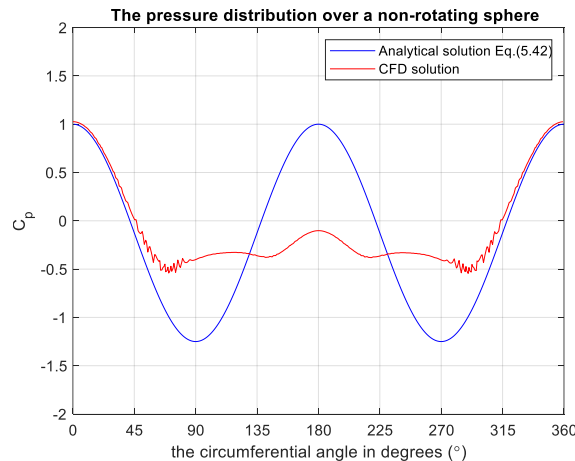


Figure 7. The Pressure Coefficient Comparison With CFD Solution For Low Viscosity Flow Around a Non-Spinning Sphere.

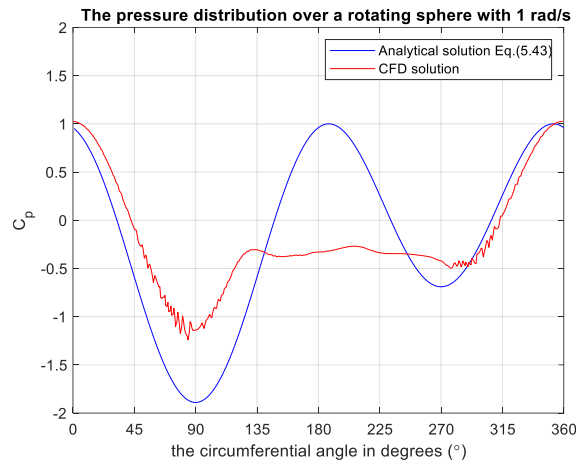


Figure 8. The Pressure Coefficient Comparison With CFD Solution For Low Viscosity Flow Around a Spinning Sphere With 1 rad/s.

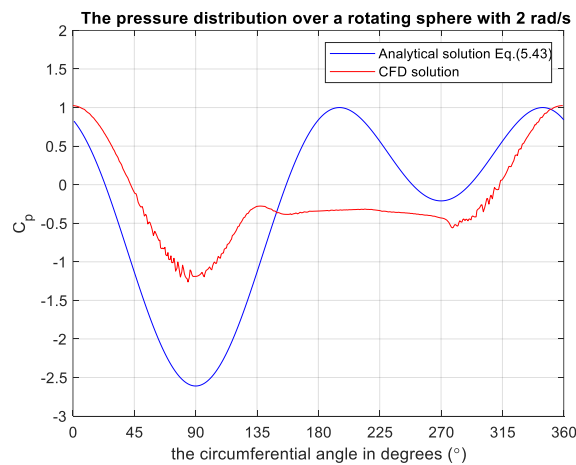


Figure 9. The Pressure Coefficient Comparison With CFD Solution For Low Viscosity Flow Around a Spinning Sphere With 2 rad/s.

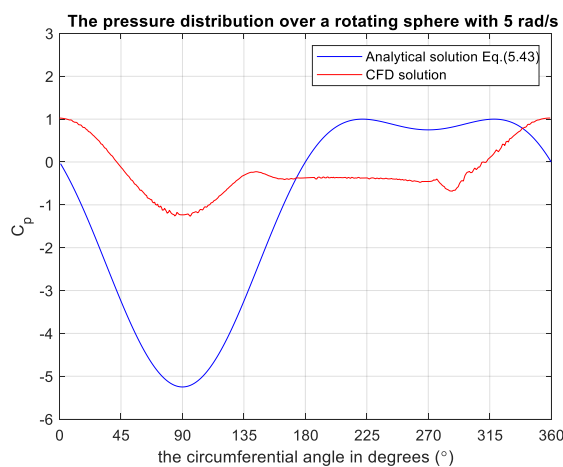


Figure 10. The Pressure Coefficient Comparison With CFD Solution For Low Viscosity Flow Around a Spinning Sphere With 5 rad/s.

In the numerical results, we can distinguish tops and bottoms, and the analytical curve of the spinning sphere achieves a qualitative agreement with the numerical results but differs quantitatively because of the viscous effect especially the separation process and the eddies formation at the rear side of the sphere.

4. Conclusion

The analytical curves of the spinning sphere achieve a qualitative agreement with the numerical results but differ quantitatively because of the viscous effect especially the separation process and the eddies formation at the rear side of the sphere.

At higher rotation rates, the flow becomes more complex. The flow field can exhibit phenomena such as separation, wake formation, and drag. Analytical solutions for the potential flow around a rotating sphere at high rotation rates are generally not available, and numerical methods such as computational fluid dynamics (CFD) are often employed to study these flows.

It's worth noting that potential flow assumptions may not accurately capture all the features of the flow around rotating spheres, especially in real-world situations where viscosity and vorticity cannot be neglected. In those cases, a more comprehensive analysis considering the effects of turbulence and boundary layers would be necessary.

CONFLICT OF INTEREST

We declare that we don't have any conflict of interest.

References

Anderson JD; Fundamentals of Aerodynamics, Sixth Edition, McGraw-Hill Book Company, 2017.

Briggs LJ; Effect of Spin and Speed on the Lateral Deflection (Curve) of a baseball; and the Magnus effects for Smooth Spheres, American Journal of Physics, 1959; 27(8), 1959: 589 -596.

F. B. Hildebrand; Advanced calculus for applications, Prentice-Hall, 1962.

F. M. White; Fluid Mechanics, 7th edition, McGraw-Hill Series in Mechanical Engineering, 2011.

Hydro-Aerodynamics Lecture Notes, Aydın ŞALCI, 2020.

L. W. Alaways , M. Hubbard; Experimental determination of baseball spin and lift, Journal of Sports Sciences, 2001, 19, 349- 358.

Mehta R. C., Aerodynamics of Spinning Sphere in Ideal Flow, Scholars Journal of Engineering and Technology (SJET), 2016; 4(5):215-219

T. Nagami, T. Higuchi, H. Nakata, T. Yanai, and K. Kanosue; Relation Between Lift Force and Ball Spin for Different Baseball Pitches, *Journal of Applied Biomechanics*, 2016, 32, 196 -204.

W.P. Graebel, *Advanced Fluid Mechanics*, Elsevier, New York, 2007